aerospace

MDPI

Article

Pressure Characteristics and Vortex Observation in Chiral-Symmetric Space Orthogonal Bifurcation

Zixuan Fang [1], Dingwei Zhang [1], Xiaokang Liu [1], Jingxuan Li [1,2], Lijun Yang [1,2] and Qingfei Fu [1,2,*]

[1] School of Astronautic, Beihang University, Beijing 102206, China; fangzx@buaa.edu.cn (Z.F.)
[2] Aircraft and Propulsion Laboratory, Ningbo Institute of Technology, Beihang University, Ningbo 315800, China
* Correspondence: fuqingfei@buaa.edu.cn

Abstract: In aerospace engine delivery systems, "one-in-two-out" bifurcation structures are commonly used for flow distribution to downstream pipelines. There are two common "one-in-two-out" bifurcation structures in aircraft engines: the planar orthogonal bifurcation and the spatial orthogonal bifurcation. By adjusting the flow supply upstream and the cross-sectional diameter downstream, the flow distribution in the two branches can be adjusted, i.e., the "splitting ratio" changes. In this paper, a dismantling and flexible experimental system is constructed to measure the pressure signals in each channel and use non-linear dynamic analysis methods to extract pressure characteristics. The particle image velocimetry (PIV) technique combined with the fine rope tracing technique is creatively used to observe the vortex structure in the cross section of the downstream branch. The study found that for spatial orthogonal bifurcation, the pressure signal characteristics in each channel are basically the same at larger splitting ratios, regardless of the chirality. As the splitting ratio decreases, the difference in pressure signal characteristics between the two branches gradually becomes evident and becomes related to the chirality. Moreover, unlike the planar orthogonal bifurcation structure, a complete large vortex structure has not been found in the downstream branch of the spatial orthogonal bifurcation structure, regardless of changes in the splitting ratio, and it is unrelated to the chirality.

Keywords: spatial orthogonal bifurcation; chirality; pressure measurement; nonlinear dynamic analysis; vortex structure

Citation: Fang, Z.; Zhang, D.; Liu, X.; Li, J.; Yang, L.; Fu, Q. Pressure Characteristics and Vortex Observation in Chiral-Symmetric Space Orthogonal Bifurcation. *Aerospace* **2023**, *10*, 568. https://doi.org/10.3390/aerospace10060568

Academic Editor: Hossein Zare-Behtash

Received: 29 April 2023
Revised: 12 June 2023
Accepted: 17 June 2023
Published: 19 June 2023

1. Introduction

The "one inlet and two outlets" bifurcation structure is widely used in fluid transportation systems. In the fields of construction, industry, and materials preparation, bifurcation structures are widely used for the distribution of water, steam, and other fluid media [1,2]. In the field of microfluidics, bifurcation structures can also be used for heat exchange assistance [3–5]. In the fields of medicine and biology, similar structures exist in the cardiovascular system [6]. In liquid rocket engines, bifurcation structures are common in propellant supply systems and play a role in flow regulation [7]. According to the relative position of the three channels, bifurcation structures can be divided into two categories: planar orthogonal bifurcation (POB, i.e., the three channels are located in the same plane, also known as "T-junction") and spatial orthogonal bifurcation (SOB, i.e., the three channels are arranged according to spatial orthogonal coordinates). The main research focus of the flow behavior in bifurcation structures is the study of pressure and vortex structures inside the pipes.

Wang et al. [8,9] built an experimental platform that closely resembles a real circular cross-section pipe system, bmeasured the pressure signals inside a T-shaped bifurcation to obtain pressure signals of flow conditions such as bubbly flow and spiral flow and conducted nonlinear dynamical analysis. Their experimental system features two branches with identical cross-sectional areas, resulting in equal flow rates within each branch during steady-state flow. The essential dimensionless parameter under investigation is the extraction rate, defined as the ratio of outlet flow rate W_3 to inlet flow rate W_1. They discovered a strong association between the disturbance behavior of pressure drop across the main and branch channels and the aforementioned parameter W_3/W_1. In practical flow processes, the cross-sectional areas of the two branches are often intentionally designed differently to meet downstream flow requirements, leading to the development of asymmetric T-junctions. In such configurations, the flow rates in the two branches are unequal, necessitating the introduction of a critical parameter: the splitting ratio, which denotes the ratio of the flow rate in branch 1 to that in branch 2. Recently, Fang et al. [10] conducted experiments to study the pressure oscillation phenomena in asymmetric T-junctions and uncovered the influence of the splitting ratio on these oscillations.

In complex and narrow spaces, such as the delivery systems of liquid rocket engines, bifurcations must be carefully arranged with a specific spatial angle to ensure proper placement. This has given rise to the development of spatial bifurcations. This study focuses on the SOB, which is the bifurcation of two branches in space that form a 90-degree angle. Our investigation has revealed a significant dearth of literature on the pressure characteristics of this type of bifurcation structure, despite its importance in the aerospace industry. Chirality is an interesting topic when it comes to space orthogonality. Chirality is observed as a functional difference between structures that can be mirrored and superimposed in space. This phenomenon is widely present in fields such as quantum chemistry, medicine, and nuclear physics [11–15]. Despite the importance of chirality in various fields, there is a lack of research exploring the impact of macroscopic chiral symmetry on fluid flow inside pipelines, especially when dealing with asymmetric branching pipelines with chiral symmetry and differing diameters. Hence, as shown in Figure 1, the main objective of this study is to examine the flow behavior in chiral-symmetric SOB.

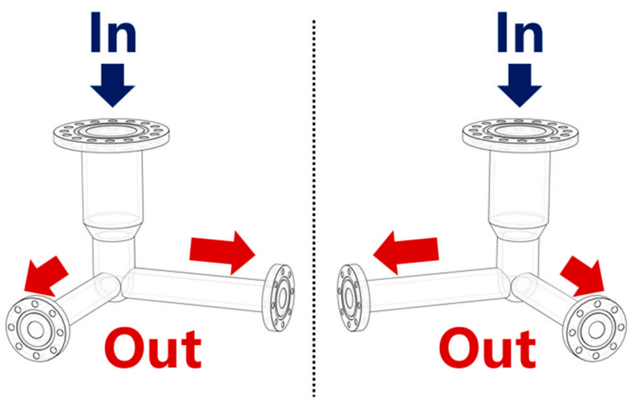

Figure 1. Schematic diagram of the space orthogonal bifurcation with handedness symmetry.

Apart from pressure characteristics, another significant flow feature in bifurcation structures is the vortex structure present in the cross-section. In recent years, there has been a large amount of experimental and numerical simulation research on internal flow in T-junctions in microfluidics. Vigolo [16] was the first to discover, through experiments, the existence of a stagnant flow region at the junction of the bifurcation in a T-junction, where low-density solid particles that pass through this region will "suspend" and remain relatively still. Vigolo believed that there is a region at the bifurcation junction that causes solid particles to stagnate within a specified range of Reynolds numbers, and the mechanism of stagnation is that two vortexes are generated at the bifurcation junction, and the reverse pressure gradient and reflux in the vortex core capture and restrict low-density solid particles near the junction. In order to clearly delineate the shape of the recirculation region, numerical simulation methods are needed to simulate the flow process. Chen [17] was the first to use the direct numeral simulation (DNS) method to study the flow in a T-junction, quantitatively describing the development of vortices inside the pipe. Ault further studied the motion trajectory of electrolyzed water bubbles at the bifurcation point of a POB at different Reynolds numbers and angles through experiments and combined the results of numerical simulation to demonstrate the existence of four recirculation regions at the bifurcation point, each recirculation region is bounded by two stagnation points (SP), one upstream and one downstream [18]. Based on the above research, Chen [19] used the same simulation method to study the flow inside a POB at different angles. Chen found that at the downstream position of the POB, outside of the recirculation region of the vortex, the streamline will form a spiral structure, called "spiral flow". He did not conduct in-depth research and explanation on this phenomenon, but this phenomenon is roughly consistent with Xiong' s computational results [20]. The experimental research on vortex structures in bifurcation structures mentioned above was mainly conducted in small-scale plane channels, and there is a significant difference between the size of the pipeline in actual transport systems and the experimental setup. The vortex behavior inside spatial bifurcation structures has not been considered. Recently, researchers have employed the PLIF (Planar Laser-Induced Fluorescence) method to visualize and study the flow field within POB at high Reynolds numbers [21]. Our research also aims to advance the research on SOB, investigating the internal flow patterns and providing insights for future studies in the aerospace field.

2. Materials and Methods

The basic experimental system of this article is illustrated in Figure 2. We built a modular experimental platform to study the pressure characteristics and cross-sectional vortex structures of SOB. In this figure, 1 is the joint module made of aluminum alloy, responsible for installing sensors and fixing devices; 2 is the diversion module made of aluminum alloy, responsible for diverting upstream fluid into two downstream branches, with internal dimensions identical to the original structure; 3 is the observation module, a glass tube made of high-transparency quartz glass; 4 is a pressure sensor fixed on the joint module; 5 is a slide rail that can easily adjust the relative position of each structural component; and 6 is a sliding block with a locking positioning device. The modules are clamped together by screws. This plan cannot observe the diversion area, but overall, it greatly reduces the shear and bending moments borne by the quartz tube and is flexible to disassemble and assemble without affecting the observation of the flow state in the downstream branch, greatly improving the efficiency of the experiment.

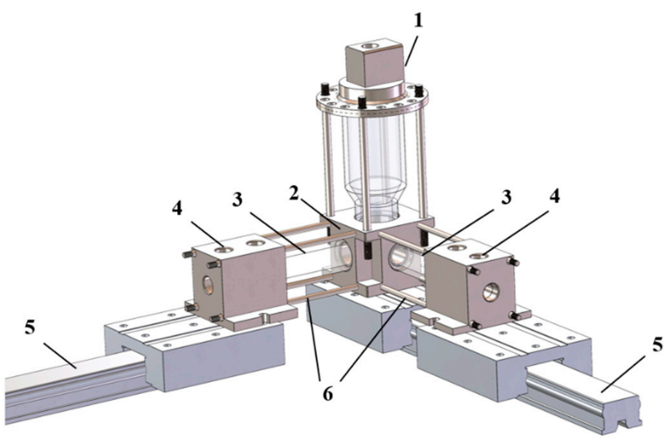

Figure 2. Schematic diagram of the experimental device for spatial orthogonal bifurcating pipeline.

The two downstream branches are selected with inner diameters of 18 mm and 22 mm to ensure the flow can reach a high Reynolds number, and defined as branch 1 and branch 2, respectively. The different inner diameters result in different flow rates in the two branches. Currently, there is no research that describes the effect of such flow rate differences on the formation and development of vortices in the SOB, nor are there any publicly available literature that shows the impact on the formation and development of vortices in the POB. The splitting ratio is defined as the ratio of the mass flow rates in the two branches:

$$\eta = \frac{\dot{m}_1}{\dot{m}_2} \tag{1}$$

In the equation, $\dot{m}_1$ is the mass flow rate of branch 1, $\dot{m}_2$ is the mass flow rate of branch 2, both of which can be directly read from the flow meter in the experimental system.

The focus of this study is the effect of flow rate ratio variation onflow behavior; and therefore, there is no need to consider the influence of surface tension. Furthermore, it is required that the working fluid has good transparency for visualization purposes and be cost-effective. Considering these factors, water was chosen as the experimental fluid, with a density of 1000 kg/m^3. The maximum valve opening of the downstream valves is 20 mm, and the feedback loop of the PLC inside the valve can control the valve opening in real-time, ensuring that the flow rates of the two branches are controlled within the given range. In the experiment, the flow rate of branch 1 is controlled at around 0.4 kg/s, and the flow rate of branch 2 varies in a relatively large range. At the same time, the pressure signals on the main branch and the two branches are collected through pressure sensors, with a sampling frequency of 5000 Hz and a sampling duration of 20 s.

In order to study the effect of chirality on the flow process, chiral symmetric components were also designed: in component 1, branch 1 and branch 2 are clockwise at a 90-degree angle, while in component 2, branch 1 and branch 2 are counterclockwise at a 90-degree angle.

3. Results and Discussion

This study focuses on investigating the influence of splitting ratio on the flow patterns within the SOB. The specific mass flow rates in each branch need to consider the maximum supply capacity of the supply system (plunger-type water pump) and the actual flow scaling in real aerospace propulsion systems. Therefore, in this study, the flow rate in branch 1 is controlled to be around 0.4 kg/s, while the flow rate in branch 2 varies between 0.2 and 0.9 kg/s. This ensures that the dimensionless splitting ratio is distributed between 0.4 and 2. By the way, the Reynolds number in each branch is defined as:

$$Re = \frac{\rho U d}{\mu} \tag{2}$$

where ρ is the density of water, U is the flow velocity in the branch, which can be obtained by measuring the mass flow rate, d is the diameter of the flow branch, and μ is the viscosity of water. After calculation, it can be found that the Reynolds numbers in both branches are of the order of 10^4, indicating turbulent flow. The Reynolds number in the smaller branch remains around 30,000, while in the larger branch, it varies between 10,000 and 50,000.

To begin with, the pressure signals in each channel under different splitting ratios were transformed into the frequency domain using FFT to perform a Fourier transform on the time-domain signals. The power spectral density (PSD) was then used to represent the vibration amplitude at various frequencies. The PSDs in each channel of both workpieces 1 and 2 under different splitting ratios are shown in Figures 3 and 4, respectively. The analysis results only retained the low-frequency range of 0–200 Hz.

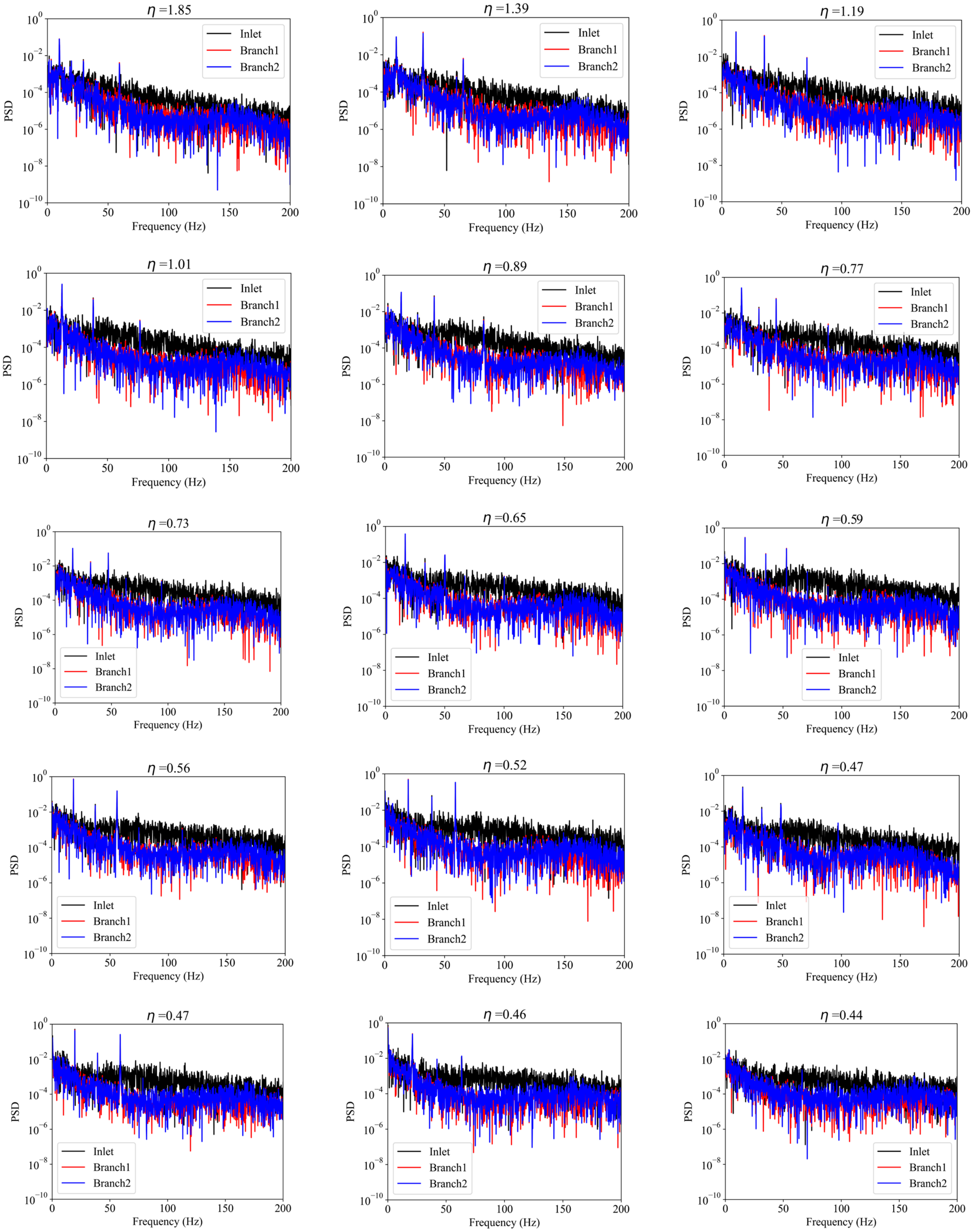

Figure 3. *Cont.*

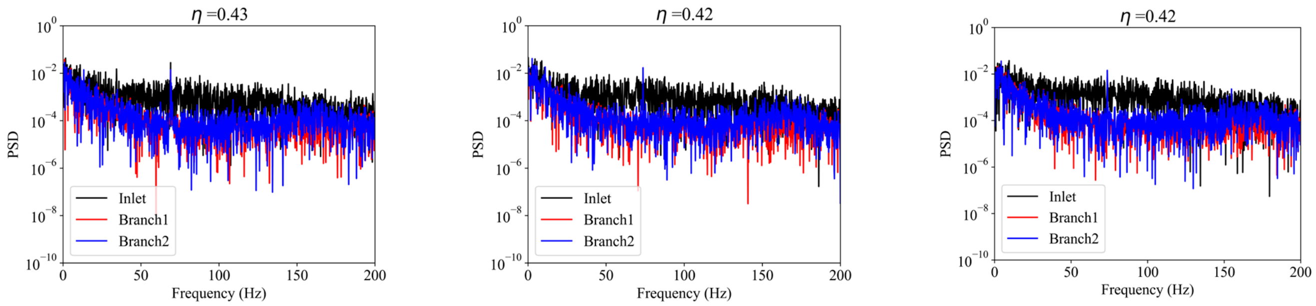

Figure 3. PSD at different splitting ratio of Workpiece 1.

The PSD of the pressure signals in different channels under different splitting ratios for Workpiece 1 is shown in Figure 3. The black, red, and blue lines in the figure represent the PSD of the pressure signals in the inlet, branch 1, and branch 2, respectively. It can be seen that the spectral signals in all three channels are generally in the form of wideband signals, with only peaks appearing near certain frequency values, and the positions of the peaks are basically the same. When the splitting ratio is above 0.5, three peaks can be observed in the frequency spectrum within 0–100 Hz, with two more prominent peaks appearing near 10 Hz and 50 Hz, and the positions of the peaks will shift to a certain extent with the change of the splitting ratio. When the splitting ratio drops below 0.5, there are basically no peaks in the main channel signal, and the peaks in both branches mainly appear near 75 Hz but are still not higher than the corresponding main channel amplitude. At the same time, the pressure amplitude in the main channel is generally higher than that in the branches. This indicates that the frequency domain characteristics of the pressure signal are closely related to the splitting ratio. A larger splitting ratio means that the flow rate in branch 1 is higher than that in branch 2, which means that more fluid enters the smaller-diameter pipe under steady-state conditions, causing the three channels of the bifurcation structure to simultaneously exhibit three "characteristic modes". As the splitting ratio decreases, the fluid entering branch 2 increases and gradually becomes dominant, which will smooth out the peaks in the main channel.

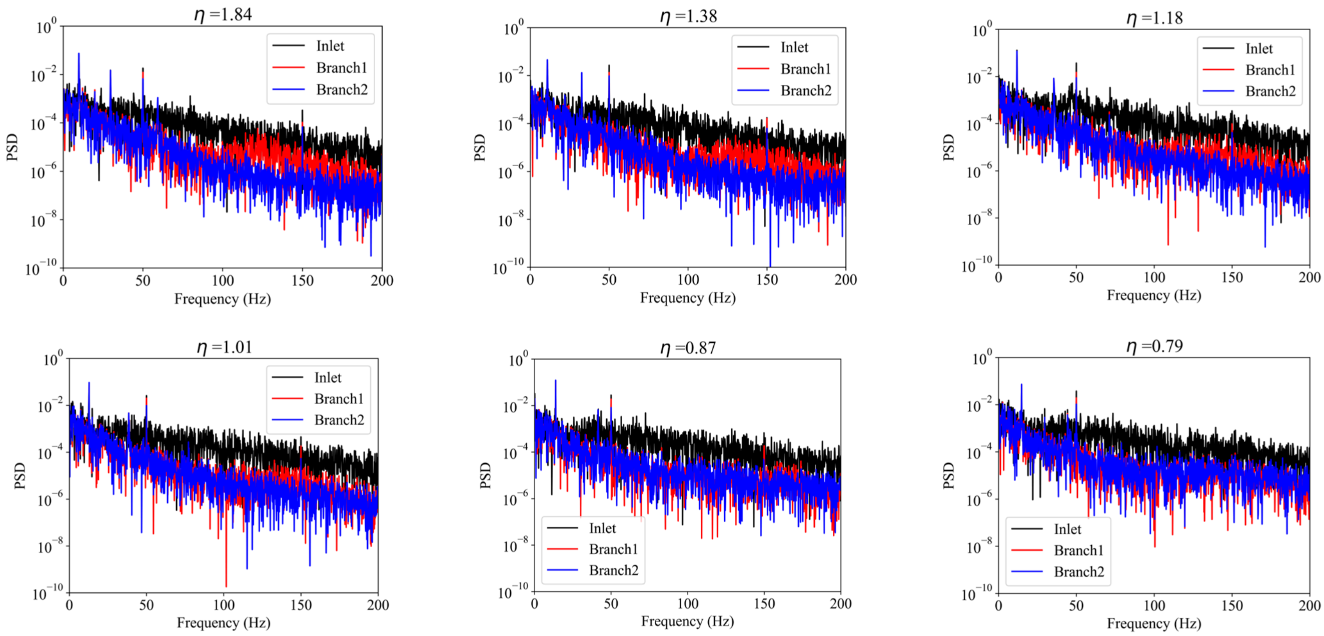

Figure 4. *Cont.*

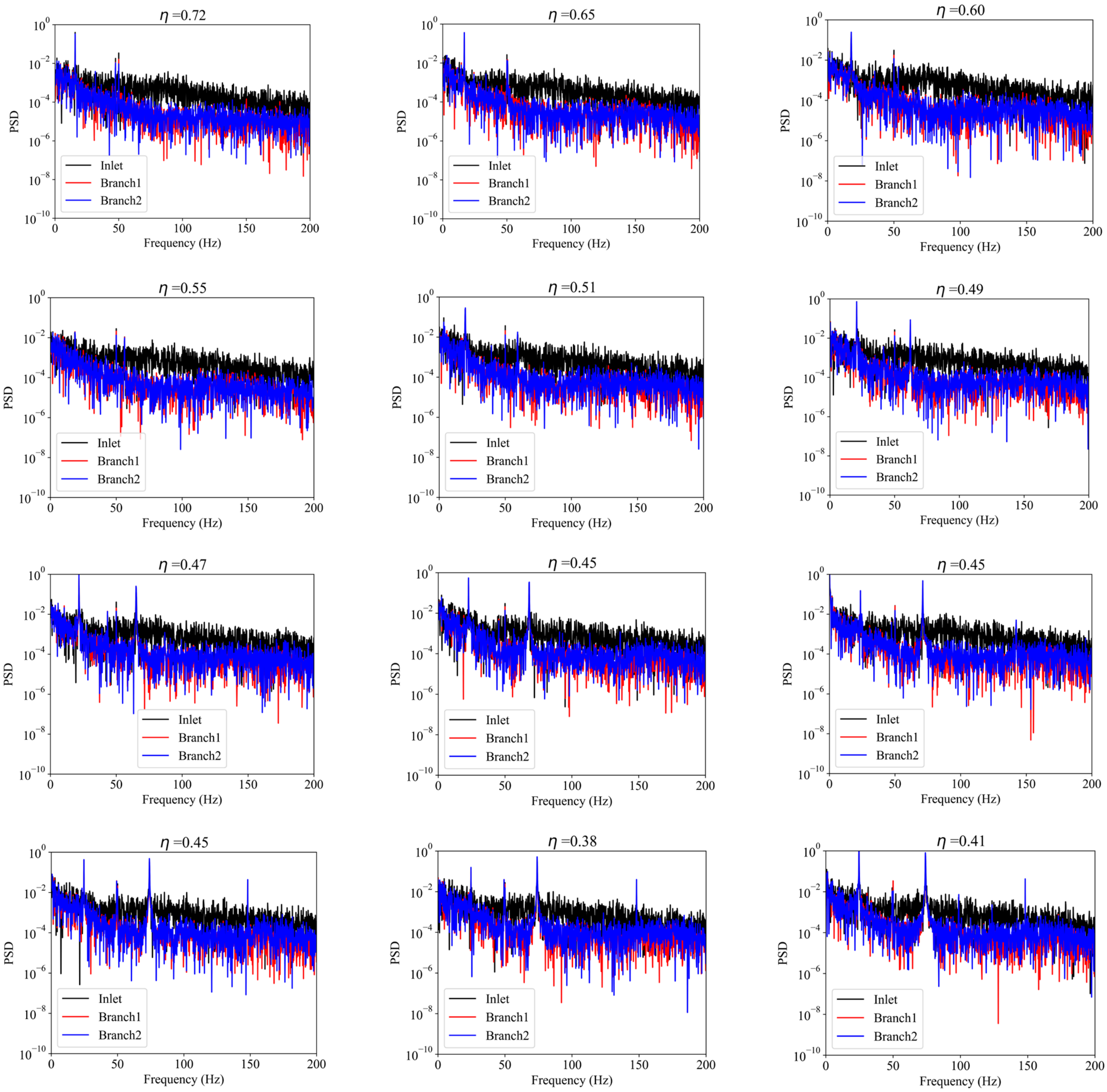

Figure 4. PSD at different splitting ratio of Workpiece 2.

As shown in Figure 4, it can be observed that Workpiece 2 also has peaks under different splitting ratios, and when the splitting ratio is above 0.5, the peaks in each channel also show a trend of being flattened. However, unlike Workpiece 1, when the splitting ratio drops below 0.5 and the flow rate in branch 2 becomes much larger than that in branch 1, the frequency spectrum signals in each channel of Workpiece 2 do not become broadband, but instead form a new peak near 70 Hz, which becomes more prominent with decreasing splitting ratio. The original peaks in each channel also do not degrade into broadband but maintain their characteristics. Obviously, the chiral structure significantly affects the pressure distribution of the flow in the spatial orthogonal bifurcation structure, and counterclockwise rotation generates more "characteristic modes" than clockwise rotation.

Figure 4 also shows that the synchronous variation of the frequency spectra in branches 1 and 2 in Workpiece 2 is weaker than that in Workpiece 1, especially when the splitting ratio is above 1. It can be seen that the pressure amplitude in branch 1 is higher than that in branch 2, which may be related to the larger flow rate in branch 1, but this degree of separation was not observed in Workpiece 1.

The above analysis was performed on the pressure signals from a statistical perspective. To further analyze the differences in the characteristics of the pressure signals, a nonlinear dynamical method is needed to study the behavior of the attractors in phase space in each channel and under different working conditions in Workpiece 1 and Workpiece 2, as shown in Figures 5 and 6. The autocorrelation function is a common statistical measure used to quantify the similarity between a signal and a delayed version of itself. It is typically calculated by multiplying the corresponding values of the signal and its delayed version, and then summing up these products over a certain range of delays. The autocorrelation function provides a more intuitive representation of the periodic characteristics of the data and serves as the basis for subsequent phase space reconstruction.

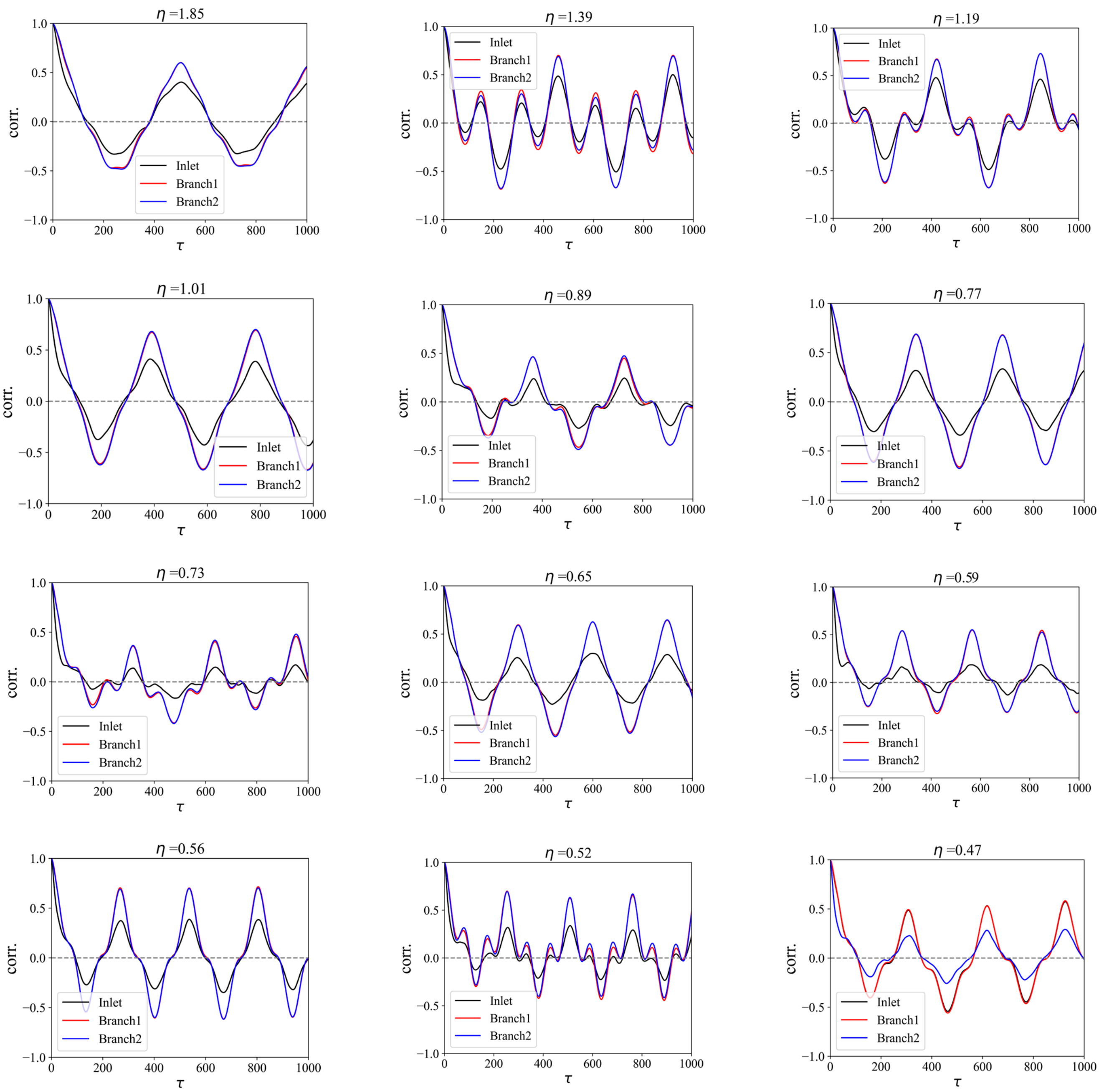

Figure 5. *Cont.*

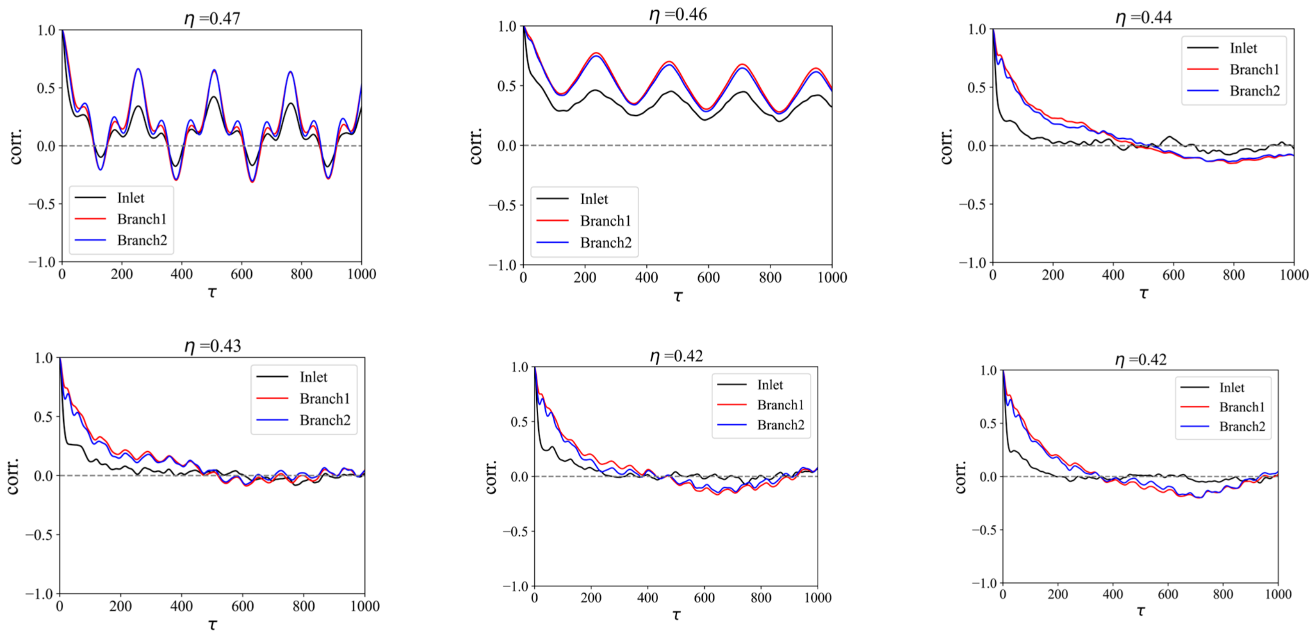

Figure 5. Autocorrelation function at different splitting ratio of Workpiece 1.

As shown in Figure 5, the results of the PSD analysis are consistent with the autocorrelation functions. The main channel and the two branches exhibit similar trends in both periodicity and amplitude, and the pressure signals in branch 1 and branch 2 show basically the same changes. When the splitting ratio is greater than 0.47, the pressure signals in different channels all exhibit good autocorrelation, with periodic crossings of the zero-scale line. When the splitting ratio decreases below 0.47, significant changes are observed in the autocorrelation of the three channels, gradually changing from periodic crossings of the zero-scale line to oscillating and decaying near the zero-scale line. The reason for this phenomenon may be that when the splitting ratio decreases to below 0.47, the attractor shape inside the dynamical system undergoes a transformation, but the specific reason still needs to be further analyzed using phase space trajectories.

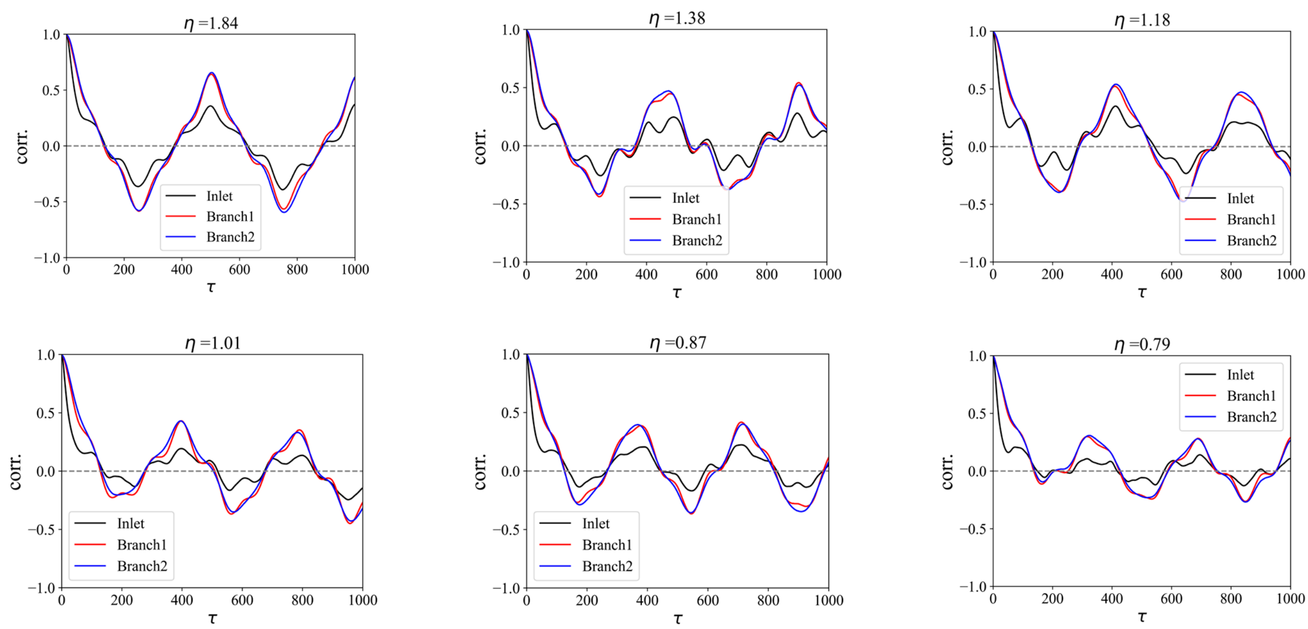

Figure 6. *Cont.*

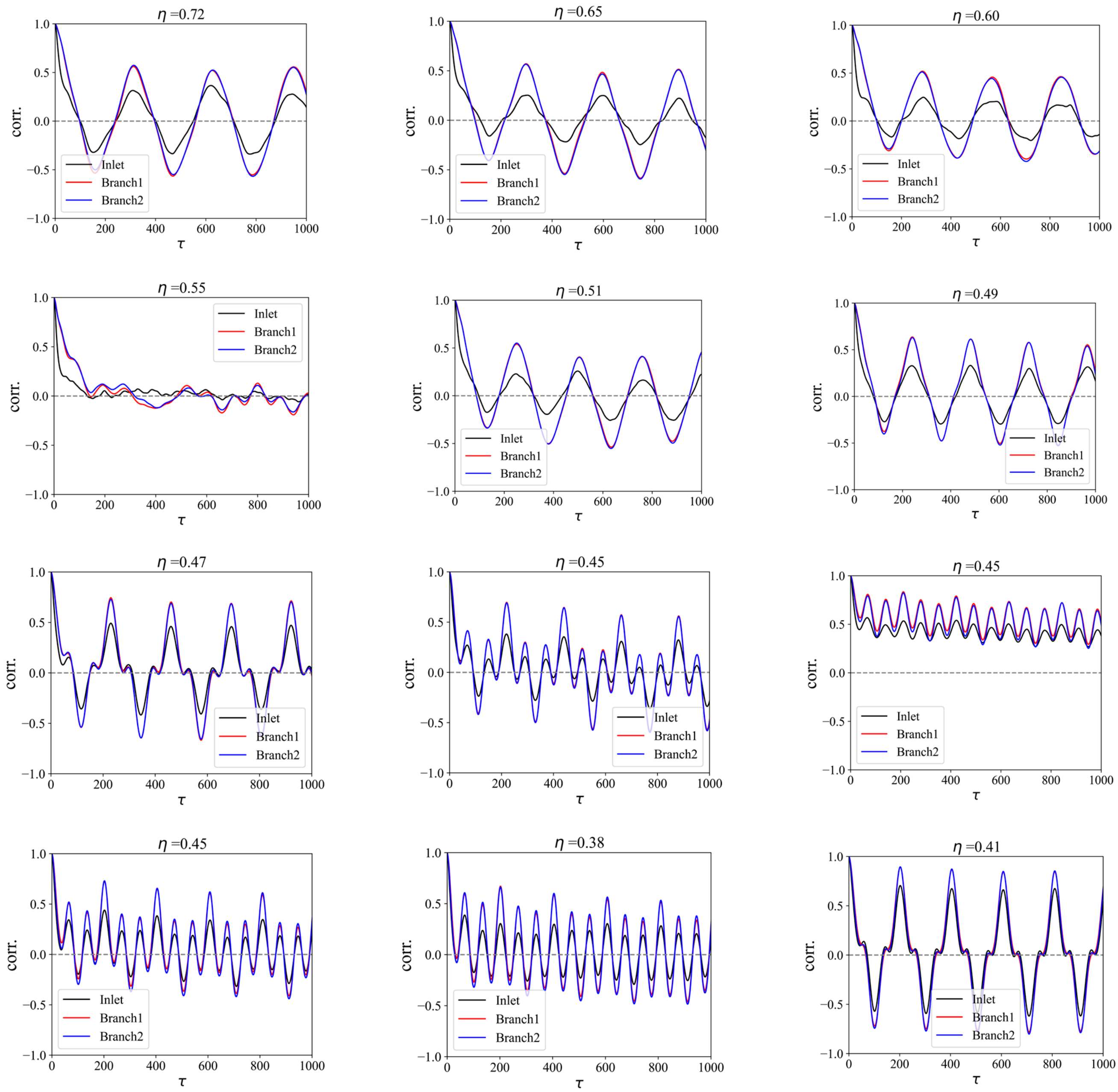

Figure 6. Autocorrelation function at different splitting ratio of Workpiece 2.

From Figure 6, it can be observed that in workpiece 2, as the split ratio decreases, the autocorrelation of the pressure signals in each channel also changes. Particularly when the split ratio is equal to 0.55, it exhibits similar oscillatory decay behavior as in workpiece 1 at small split ratios. However, unlike workpiece 1, the autocorrelation signals in workpiece 2 continue to exhibit strong periodicity below a split ratio of 0.5 instead of oscillatory decay. Similar to the PSD signals, the autocorrelation functions of the two branches in workpiece 2 also do not exhibit complete synchronization when the split ratio is large, and their difference is much more significant than in workpiece 1. However, with the increase in flow rate in branch 2, their synchronization is corrected.

After obtaining the autocorrelation functions, in order to achieve the optimal visualization effect of the phase space trajectory, the time delay is usually selected as the value corresponding to the first crossing of the zero-scale line in the autocorrelation function. In this paper, the time delay is uniformly selected as 200. The reconstructed phase space trajectories of workpiece 1 and workpiece 2 are shown in Figures 7 and 8, respectively.

In Figure 7, it can be observed that the attractor shapes of the pressure signals in the three channels are similar in phase space, with the attractor volume of the main channel being significantly larger than that of the two branch channels, which is related to the larger pressure fluctuations in the main channel. When the flow split ratio is relatively large, the positions of the attractors in the phase space of the three channels can be clearly observed: branch 2 is located between the main channel and Branch 1, with a lower flow rate in Branch 2. However, as the flow split ratio decreases, the phase space trajectory of branch 2 gradually approaches that of branch 1, and when the flow split ratio is around 0.5, the two trajectories completely overlap. The figure also shows that when the flow split ratio is 0.46, the attractors of the main channel and the two branch channels are all affected to some extent, but they all return to their previous shapes at smaller flow split ratios.

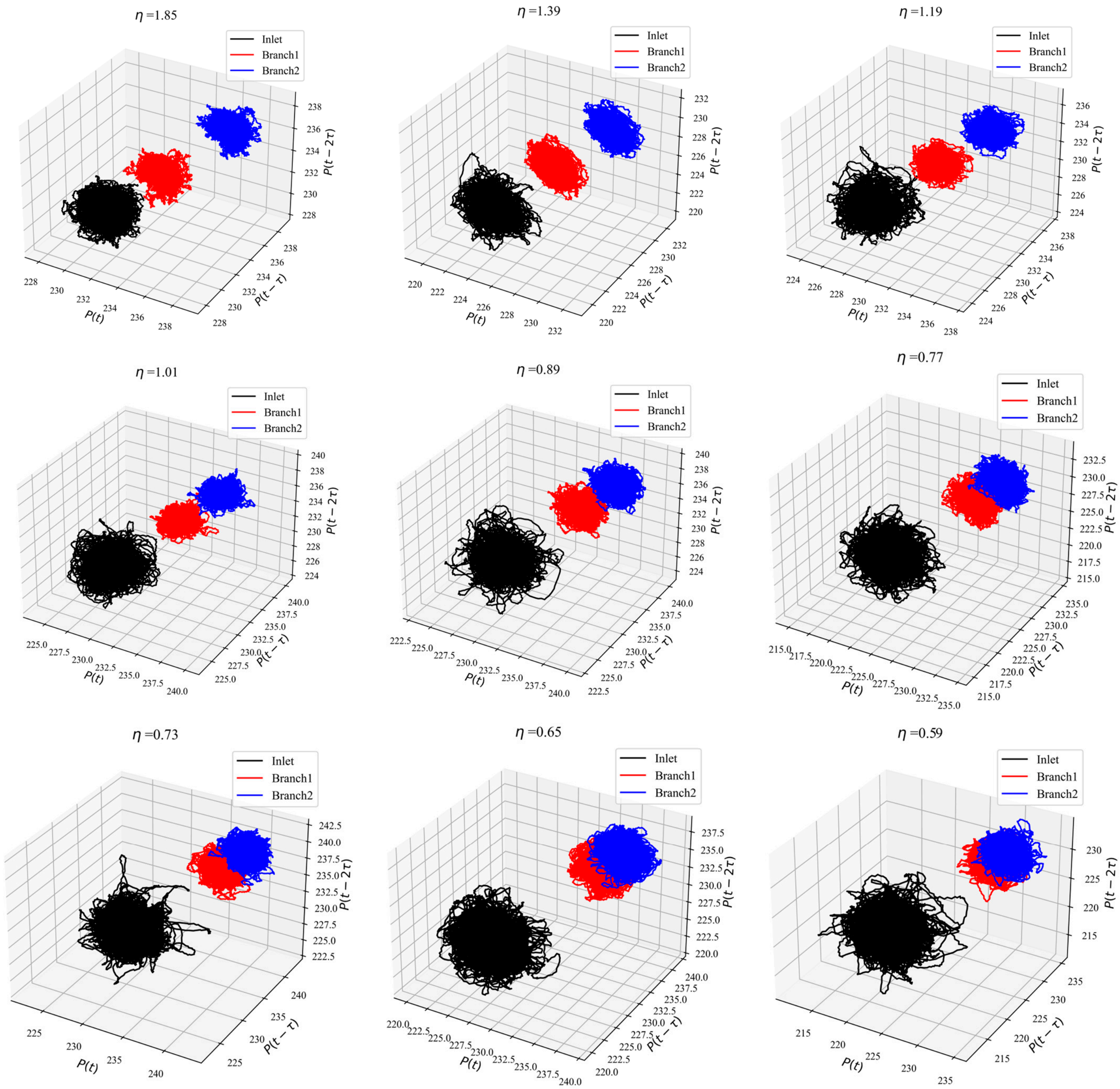

Figure 7. *Cont.*

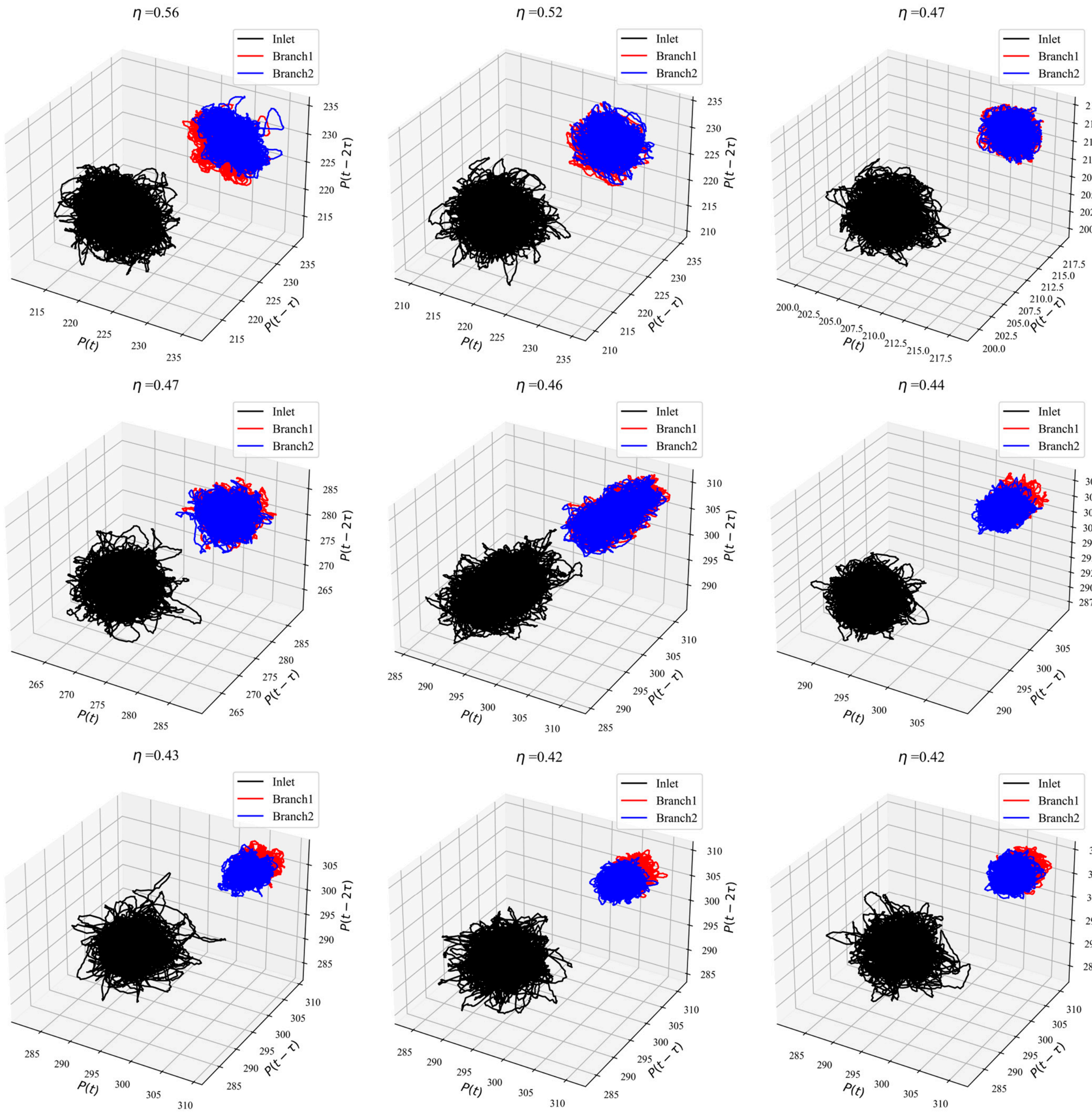

Figure 7. Phase space trajectories at different splitting ratio of Workpiece 1.

In Figure 8, it can be observed that the arrangement of attractors in the phase space of Workpiece 2 is similar to that of Workpiece 1 when the bifurcation ratio is relatively large: the attractor volume of the main channel is the largest, and the attractor of branch 2 is located between the two. Similarly, as the bifurcation ratio decreases, the attractor of branch 2 will move closer to branch 1. However, when the bifurcation ratio decreases to around 0.45, it can be observed that the shapes of all three attractors are stretched, and the shape of the attractor of branch 2 is stretched to span across the main channel and branch 1. To verify whether the above phenomenon actually occurs, the method of constructing a Poincaré section can be adopted to study the trajectory of the high-dimensional dynamical system in a low-dimensional space. Following the description by Kantz et al. in their monograph [22], the phase space trajectories and Poincaré sections complement each other as high-dimensional and low-dimensional features of the dynamical system, respectively, providing a more comprehensive representation of the system's characteristics. Hence, they are jointly presented in the paper. The Poincaré sections of the pressure signals in each channel of Workpiece 1 and Workpiece 2 under different bifurcation ratios are shown in Figures 9 and 10.

The results of the Poincaré sections in Figures 9 and 10 confirm the phenomena observed in the phase space trajectories. The attractors in both workpieces 1 and 2 do exhibit changes with the variation of the flow ratio. This is related to the different angles of the bifurcation in the two workpieces. In the flow process, the fluid is subject to different inertial forces in different directions, leading to different oscillation phenomena within the bifurcation, and causing differences in the pressure signals.

To visualize the vortex structures in spatially orthogonal bifurcations and planar orthogonal bifurcations, the PIV technique was used to observe the cross-sections. The colormap represents the magnitude of vorticity, while the arrows indicate velocity vectors. The results show that in POB, at certain flow split ratios, the formation and breakdown of larger vortex structures, as shown in Figure 11a, can be observed. However, in SOB, only flow behavior with non-uniform vorticity distribution, as shown in Figure 11b, can be observed in both branches, but the formation and breakdown of vortex structures are absent.

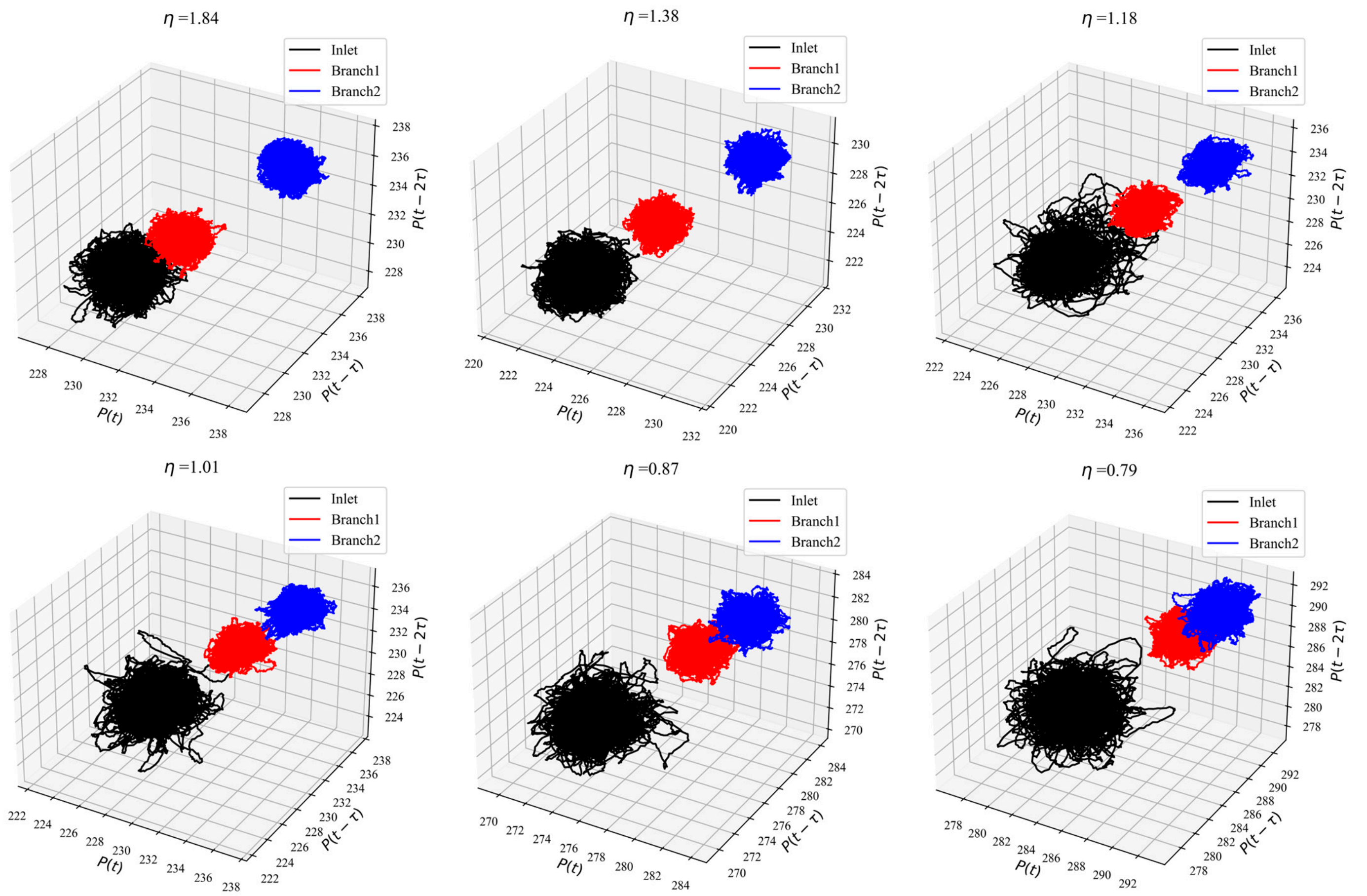

Figure 8. *Cont.*

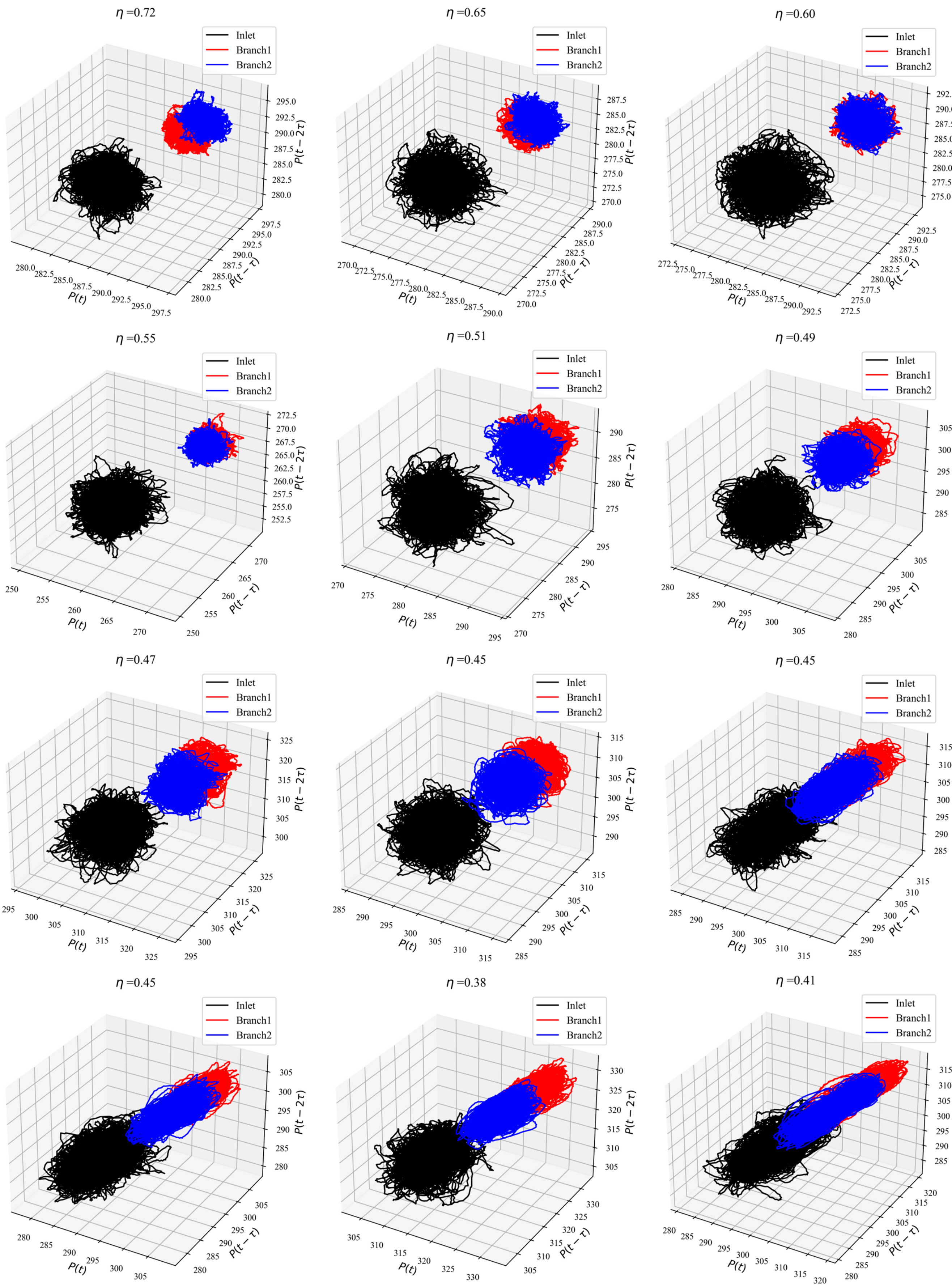

Figure 8. Phase space trajectories at different splitting ratio of Workpiece 2.

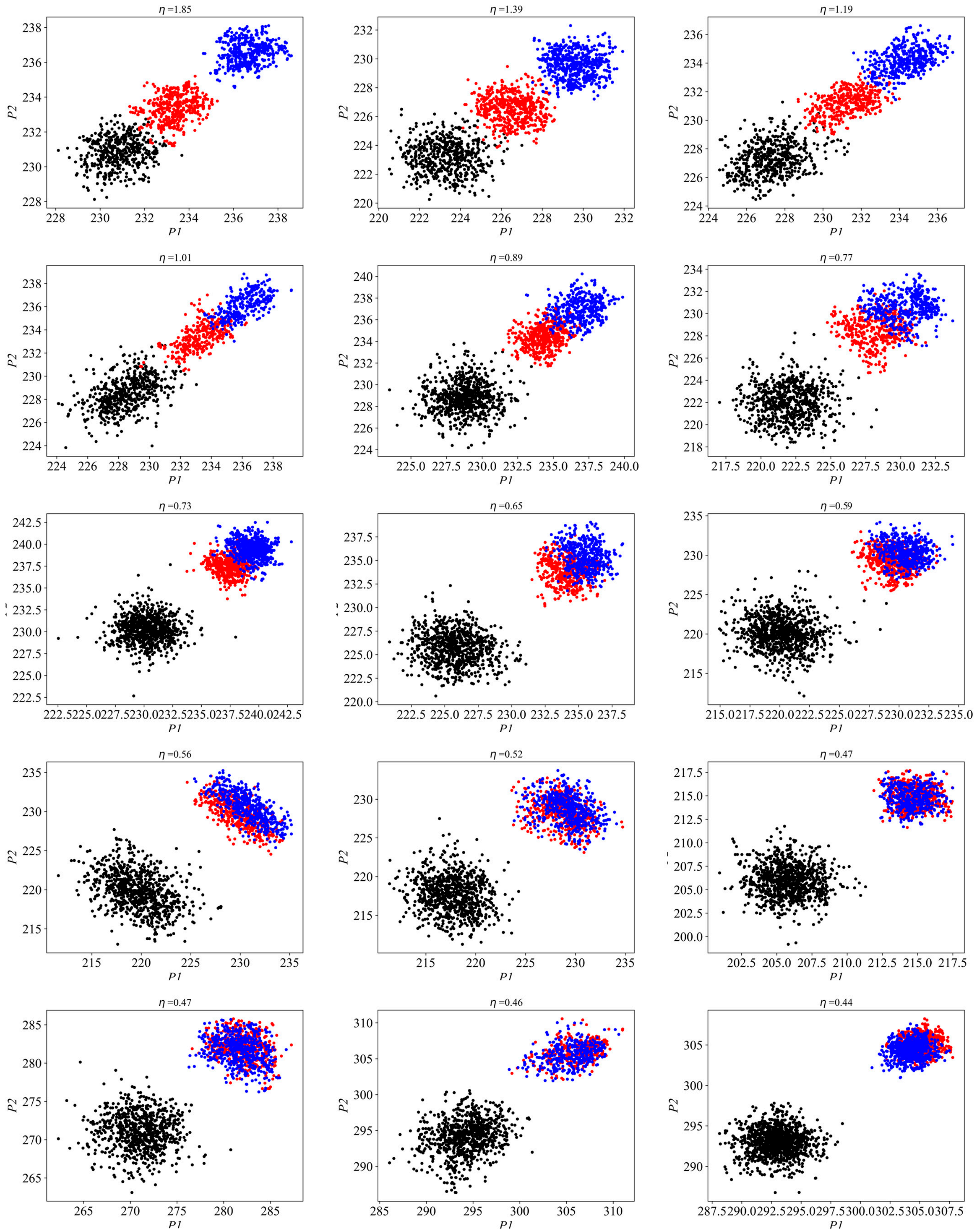

Figure 9. *Cont.*

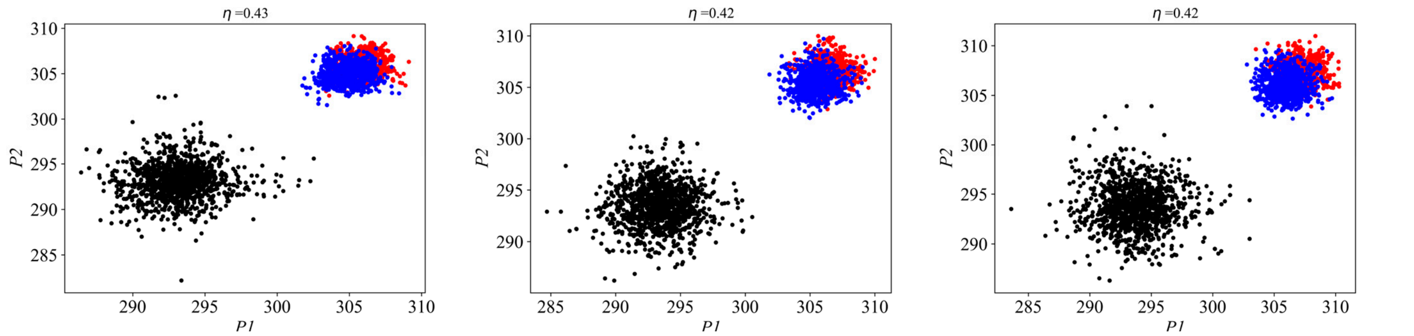

Figure 9. Poincaré sections at different splitting ratio of workpiece 1.

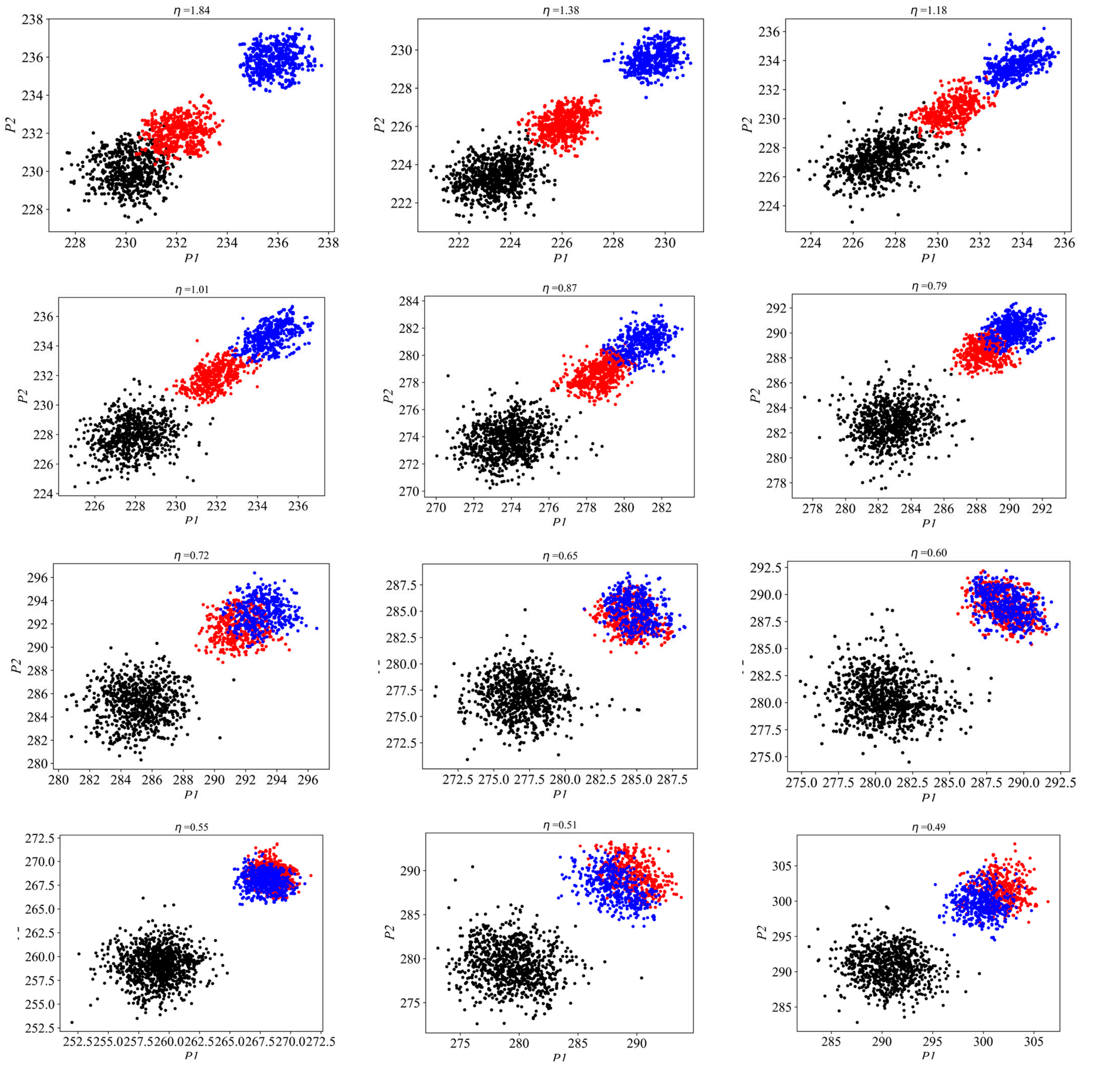

Figure 10. *Cont.*

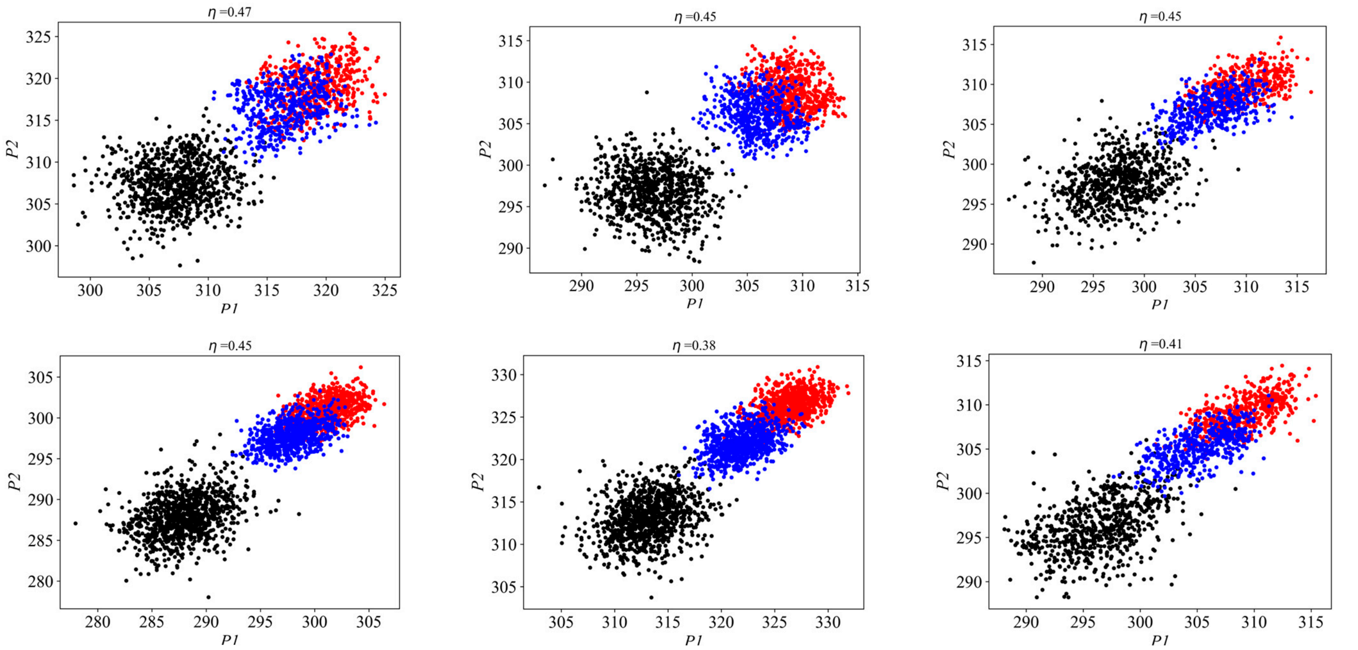

Figure 10. Poincaré sections at different splitting ratio of workpiece 2.

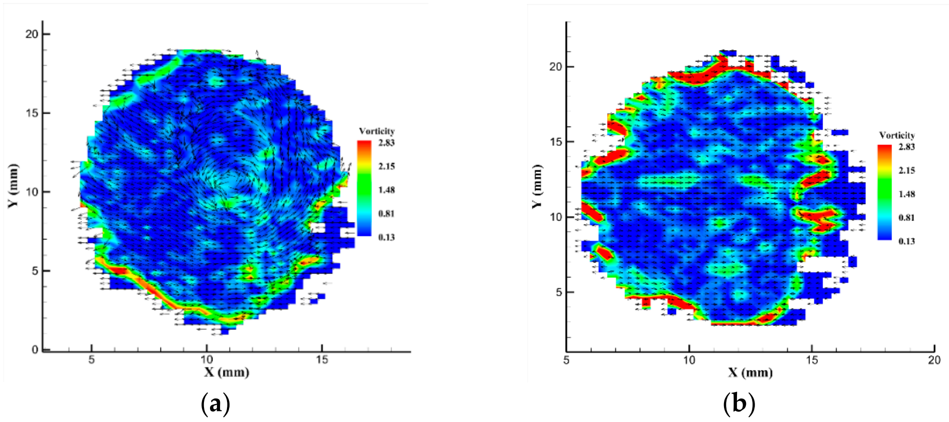

Figure 11. Cross-sectional (**a**) with vortex structures (T-shaped) and (**b**) without vortex structures (SOB).

To simplify the observation process and verify the results obtained from PIV, a string-tracing method was used to observe the number of times the string wraps around in the branch. The basic principle of this technique can be found in Fang et al. [10]. The biggest advantage of using this technique is that it makes it very easy to observe the generation of vortex structures inside the branches. The study showed that in the POB, the strings in branch 1 and branch 2 exhibit a wrapping phenomenon under specific flow conditions, as shown in Figure 12a. However, in the SOB, the behavior of the strings in branch 1 and branch 2 is as shown in Figure 12b.

Based on the PIV and string-tracing results, it can be concluded that the vortex structures in the downstream branches only occur in the POB and are not affected by chirality. This suggests that, compared to the POB, the space orthogonal bifurcation can suppress the formation of vortex structures in the downstream branches. However, the specific mechanism still requires further investigation.

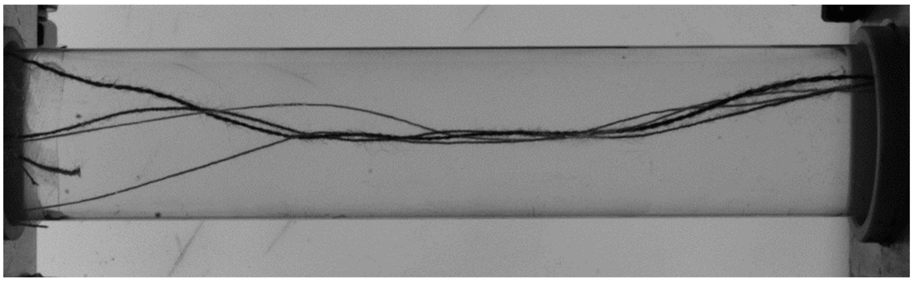

(**a**)

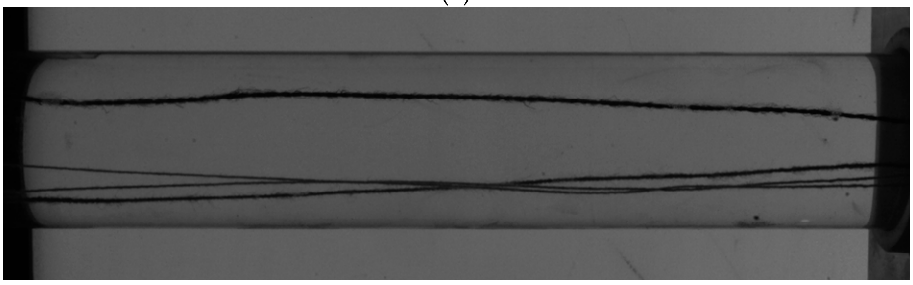

(**b**)

Figure 12. String-tracing results (**a**) with vortex structure and (**b**) without vortex structure.

4. Conclusions

We constructed a split-type experimental system to investigate the flow behavior inside a chiral symmetric spatial orthogonal bifurcation and measured the pressure signals and vortex formation patterns at a certain cross-section in each channel. Our study revealed the following findings:

1. Chirality structure affects the pressure signal characteristics inside the spatial orthogonal bifurcation, especially when the bifurcation ratio is smaller than 0.5. This effect can be observed in the frequency spectrum, autocorrelation function, phase space trajectory, and Poincaré section. This phenomenon may be related to the different directions of inertial forces.
2. The SOB structure eliminates the large vortex structure in the downstream branch. Through PIV technology and fine wire tracing technology, the vortex structure observed in the planar orthogonal bifurcation cannot be observed in the spatial orthogonal bifurcation. The mechanism behind this phenomenon is not yet fully understood and requires further research at the mechanism level.

This study first investigates the flow behavior of chiral symmetric SOB under different bypass ratios, taking into account the practical engineering background. It provides a comprehensive examination and serves as a reference for future research.

Author Contributions: Conceptualization, Z.F. and Q.F.; methodology, D.Z.; software, X.L.; validation, Z.F., D.Z. and X.L.; formal analysis, X.L.; investigation, Z.F.; resources, D.Z.; data curation, X.L.; writing—original draft preparation, Z.F.; writing—review and editing, Z.F.; visualization, D.Z.; supervision, Q.F.; project administration, Q.F. and L.Y.; funding acquisition, J.L. All authors have read and agreed to the published version of the manuscript.

Funding: This research was supported by the National Natural Science Foundation of China (grant No. 11272026, 11922201, 11927802).

Data Availability Statement: The datasets generated and/or analyzed during the current study are not publicly available due to the need to protect intellectual property rights. However, the datasets are available from the corresponding author on reasonable request. Access to the data will be granted in accordance with any institutional or ethical requirements.

Acknowledgments: The authors would also like to thank Penghui Li, Wentong Qiao, Hu Sun, and Qixiang Gao for their assistance.

Conflicts of Interest: The authors declare no conflict of interest.

References

1. McDonald, C.J.; Devon, M.J. Hollow latex particles: Synthesis and applications. *Adv. Colloid Interface Sci.* **2002**, *99*, 181–213. [CrossRef]
2. Seymour, R.B. The role of fillers and reinforcements in plastics technology. *Polym. Plast. Technol. Eng.* **1976**, *7*, 49–79. [CrossRef]
3. Dreher, S.; Kockmann, N.; Woias, P. Characterization of laminar transient flow regimes and mixing in T-shaped micromixers. *Heat Transf. Eng.* **2009**, *30*, 91–100. [CrossRef]
4. Senn, S.M.; Poulikakos, D. Laminar mixing, heat transfer and pressure drop in tree-like microchannel nets and their application for thermal management in polymer electrolyte fuel cells. *J. Power Sources* **2004**, *130*, 178–191. [CrossRef]
5. Kockmann, N.; Engler, M.; Haller, D.; Woias, P. Fluid Dynamics and Transfer Processes in Bended Microchannels. *Heat Transf. Eng.* **2005**, *26*, 71–78. [CrossRef]
6. Meng, H.; Wang, Z.; Hoi, Y.; Gao, L.; Metaxa, E.; Swartz, D.; Kolega, J. Complex Hemodynamics at the Apex of an Arterial Bifurcation Induces Vascular Remodeling Resembling Cerebral Aneurysm Initiation. *Stroke* **2007**, *38*, 1924–1931. [CrossRef]
7. Casiano, M.J.; Hulka, J.R.; Yang, V. Liquid-Propellant Rocket Engine Throttling: A Comprehensive Review. *J. Propuls. Power* **2010**, *26*, 897–923. [CrossRef]
8. Wang, S.; Shoji, M. Fluctuation characteristics of two-phase flow splitting at a vertical impacting T-junction. *Int. J. Multiph. Flow* **2002**, *28*, 2007–2016. [CrossRef]
9. Wang, S.; Mosdorf, R.; Shoji, M. Nonlinear analysis on fluctuation feature of two-phase flow through a T-junction. *Int. J. Heat Mass Transf.* **2003**, *46*, 1519–1528. [CrossRef]
10. Fang, Z.X.; Li, Y.J.; Zhang, D.W.; Liu, X.K.; Li, J.X.; Yang, L.J.; Fu, Q.F. Pressure Oscillation and Vortex in an Asymmetric T-junction. *Acta* **2023**. *Submitted*.
11. Liu, H.R.; Li, H.P.; He, Y.; Cheng, P.; Zhang, Y.Q.; Feng, B.; Li, H.; Wu, K.; Chen, L. Condensation and asymmetric amplification of chirality in achiral molecules adsorbed on an achiral surface. *Nat. Commun.* **2023**, *14*, 2100. [CrossRef]
12. Hentschel, M.; Schäferling, M.; Duan, X.Y.; Liu, N. Chiral plasmonics. *Sci. Adv.* **2017**, *3*, e1602735. [CrossRef] [PubMed]
13. Fukushima, K.; Kharzeev, D.E.; Warringa, H.J. Chiral magnetic effect. *Phys. Rev. D* **2008**, *78*, 074033. [CrossRef]
14. Diakonov, D.; Petrov, V.; Pobylitsa, P. A chiral theory of nucleons. *Nucl. Phys. B* **1988**, *306*, 809–848. [CrossRef]
15. Pisarski, R.D.; Wilczek, F. Remarks on the chiral phase transition in chromodynamics. *Phys. Rev. D* **1984**, *29*, 338–341. [CrossRef]
16. Vigolo, D.; Radl, S.; Stone, H.A. Unexpected trapping of particles at a T junction. *Proc. Natl. Acad. Sci. USA* **2014**, *111*, 4770–4775. [CrossRef] [PubMed]
17. Chen, K.K.; Rowley, C.W.; Stone, H.A. Vortex dynamics in a pipe T-junction: Recirculation and sensitivity. *Phys. Fluids* **2015**, *27*, 034107. [CrossRef]
18. Ault, J.T.; Fani, A.; Chen, K.K.; Shin, S.; Gallaire, F.; Stone, H.A. Vortex-breakdown-induced particle capture in branching junctions. *Phys. Rev. Lett.* **2016**, *117*, 084501. [CrossRef] [PubMed]
19. Chen, K.K.; Rowley, C.W.; Stone, H.A. Vortex breakdown, linear global instability and sensitivity of pipe bifurcation flows. *J. Fluid Mech.* **2017**, *815*, 257–294. [CrossRef]
20. Xiong, A.; Wei, Q. Experiment study on a sort of strong swirling flow. *Exp. Meas. Fluid Mech.* **1999**, *13*, 8–13. (In Chinese)
21. Su, B.; Huang, K.; Lin, M.; Wang, Q. Experimental investigation on the flow patterns in a T-junction under steady and rolling motion conditions using PLIF. *Chem. Eng. J.* **2023**, *465*, 142772. [CrossRef]
22. Kantz, H.; Schreiber, T. *Nonlinear Time Series Analysis*, 2nd ed.; Cambridge University Press: Cambridge, UK, 2004.